Contribution from the Institute for Inorganic Chemistry, University of Witten/Herdecke, Stockumer Strasse 10, 5810 Witten-Annen, Federal Republic of Germany

Kinetics and Mechanism of the Formation of Fe^{II}(edta)NO in the System Fe^{II}(edta)/NO/HONO/NO_2^- in Aqueous Solutions

V. Zang, M. Kotowski, and R. van Eldik*

Received March 18, 1988

NO, HONO, and NO_2^- react with Fe^{II}(edta) in aqueous solution to produce Fe^{II}(edta)NO. The reaction with NO is too fast for conventional stopped-flow and *T*-jump techniques, whereas the reaction with HONO/NO_2^- can be followed kinetically by using stopped-flow techniques. This reaction occurs in two parallel paths of different order, viz. pseudo first and pseudo zero order in Fe^{II}(edta) concentration, respectively. The contribution of each path strongly depends on the pH and total nitrite concentration employed. The kinetics of the reaction can be described by the rate law $-d[Fe^{II}(edta)]/dt = k_a[HONO]^2 + k_b[Fe^{II}(edta)][HONO]$, where k_a and k_b have the values 62 ± 12 and 90 ± 16 M^{-1} s^{-1}, respectively, at 25 °C and 0.5 M ionic strength. The suggested mechanism involves the rate-determining formation of NO^+ and the reduction of HONO to NO by Fe^{II}(edta), to account for the parallel reaction paths. The results are discussed in comparison to the available literature data.

Introduction

Our interest in the absorption and subsequent redox reactions of NO_x (i.e. NO and its oxidation products) in aqueous solution was stimulated by some recent reports on catalytic cycles for the removal of NO_x from flue gases of coal-fired power plants. Of particular interest are systems in which simultaneous removal of SO_2 and NO_x result in the oxidation of sulfite and reduction of NO_x. In such processes, metal chelates are used to bind NO in order to improve the absorption degree (NO is almost insoluble in H_2O) and to catalyze the redox process.[1-7] In addition, the aqueous chemistry and catalytic role of metal ions are in general of considerable importance in atmospheric oxidation processes of S(IV).[8,9] The role of NO_x species in such processes and their interaction with metal ions and complexes are therefore of fundamental interest to environmental chemistry, especially in terms of the acid rain phenomenon.[10]

The mechanistic detail of such metal-catalyzed processes is to a large extent unknown. In this paper we report our mechanistic findings for the reaction of NO_x (i.e. NO, HONO, and NO_2^-) with the potential catalyst Fe^{II}(edta), where edta = ethylenediaminetetraacetate. This catalyst exhibits interesting properties for the simultaneous removal of SO_2 and NO_x from flue gases.[4-7] After completion of our work, a report on the reaction of NO_2^- with Fe^{II}(edta) appeared in the literature.[11] A comparison of the reported data with those of the present study is made. It is furthermore important to note that there has been much interest lately in the reduction of nitrite by various complexes of Mo(V), Co(III), Fe(II), and Cr(II),[12-19] which involve reactions similar to those investigated in this study.

Experimental Section

Materials. Chemicals of analytical reagent grade and deionized water were used throughout this study. Fe^{II}(edta) was prepared in solution from $FeSO_4$ and $Na_2(H_2edta)$. Acetic acid/sodium acetate buffers were used to control the pH of the test solution, and Na_2SO_4 was used to adjust the ionic strength of the medium.

Preparation of Solutions. Preliminary studies demonstrated that Fe^{II}(edta) is extremely oxygen-sensitive and is rapidly oxidized to Fe^{III}(edta). In order to avoid this complication, all Fe^{II}(edta) solutions were prepared in the absence of O_2. A stock solution of $Na_2(H_2edta)$ containing Na_2SO_4 (to adjust the ionic strength) was degassed on a vacuum line and washed a few times with O_2-free argon (O_2 removed over a catalyst), before the Fe(II) salt was added. The colorless Fe^{II}(edta) solution so prepared remained stable for up to 6 h before a noticeable color change (monitored spectrophotometrically) indicated the partial formation of Fe^{III}(edta). The buffer solutions were degassed in a similar way before addition of $NaNO_2$ or NO gas. These solutions were transferred with the aid of gastight syringes to the stopped-flow unit or spectrophotometer cells. Blank experiments indicated that no O_2 entered the test solutions during the chosen handling procedure.

The Fe^{II}(edta)NO complex was prepared in solution by passing O_2-free NO gas through an evacuated solution of Fe^{II}(edta). The reaction goes to completion within a few minutes, required to dissolve the NO gas. The buffer concentration was kept as low as possible in order to eliminate possible side reactions. Furthermore, the buffer components were always added to the NO or NO_2^- stock solution prior to mixing with Fe^{II}(edta). Control experiments indicated that the buffer components had no significant effect on the observed kinetics. The pH of the reaction mixture was measured on a Metrohm 632 pH meter (Sigma glass electrode) directly connected to the receiver syringe of the stopped-flow instrument.

Kinetic Measurements. UV–vis spectra and slow kinetic measurements were performed in gastight cuvettes in the thermostated (±0.1 °C) cell compartment of a Shimadzu UV 250 spectrophotometer. Faster reactions were studied on a modified, thermostated (±0.1 °C) Aminco stopped-flow instrument that operates in a double-beam mode to reduce the base-line noise resulting from fluctuations in the xenon lamp intensity. Absorbance/time traces were recorded on a Dasar transient recorder and transferred to an on-line computer for the calculation of the rate constants. Under certain experimental conditions parallel zero- and first-order reactions were observed and a special procedure was developed to treat such data on an Atari Mega 4 computer. Some preliminary measurements were also performed on a Göttingen Messanlagen *T*-jump instrument.

Results and Discussion

Preliminary Observations. Solutions of Fe^{II}(edta) are rapidly oxidized by O_2 to Fe^{III}(edta). Stopped-flow measurements revealed a rate constant of (2.3 ± 0.2) × 10^3 M^{-1} s^{-1} for this reaction at 25 °C and pH 2.5. This rate constant reduces to 80 M^{-1} s^{-1} at pH 5. The formation of Fe^{III}(edta) is accompanied by a significant increase in absorbance around 400 nm. It is therefore absolutely necessary to work under O_2-free conditions in order to be able

(1) Schrod, M.; Semel, J.; Steiner, R. *Chem.-Ing.-Tech.* **1985**, *57*, 717.
(2) Weisweiler, W.; Retzlaff, B.; Raible, L. *Chem. Eng. Process.* **1984**, *18*, 85.
(3) Chang, S. G.; Littlejohn, D.; Lynn, S. *Environ. Sci. Technol.* **1983**, *17*, 649.
(4) Sada, E.; Kumazawa, H.; Kudo, I.; Kondo, T. *Ind. Eng. Chem. Process Des. Dev.* **1980**, *19*, 377.
(5) Sada, E.; Kumazawa, H.; Takada, Y. *Ind. Eng. Chem. Fundam.* **1984**, *23*, 60.
(6) Sada, E.; Kumazawa, H.; Hiskosaka, H. *Ind. Eng. Chem. Fundam.* **1986**, *25*, 386.
(7) Sada, E.; Kumazawa, H.; Machida, H. *Ind. Eng. Chem. Res.* **1987**, *26*, 2016.
(8) Chang, S. G.; Littlejohn, D.; Hu, K. Y. *Science (Washington, D.C.)* **1987**, *237*, 756 and literature cited therein.
(9) van Eldik, R. In *Chemistry of Multiphase Atmospheric Systems*; Jaeschke, W., Ed.; Springer-Verlag: West Berlin 1986; p 541.
(10) Sigg, L.; Stumm, W.; Zobrist, J.; Zürcher, F. *Chimia* **1987**, *41*, 159.
(11) Shearer, D. S. Ph.D. Dissertation, Virginia Polytechnic Institute and State University, Blacksburg, VA, 1984; *Chem. Abstr.* **1986**, *104*, 156577v.
(12) Hishinuma, Y.; Kayi, R.; Akimoto, H.; Nakajima, F.; Mori, T.; Kamo, T.; Arikawa, Y.; Nozawa, S. S. *Bull. Chem. Soc. Jpn.* **1979**, *52*, 2863.
(13) Ogino, H.; Tukahara, K.; Tanaka, N. *Bull. Chem. Soc. Jpn.* **1974**, *47*, 2863.
(14) Melton, J. D.; Bakac, A.; Espenson, J. H. *Inorg. Chem.* **1986**, *25*, 3360.
(15) Hayde, M. R.; Garner, C. D. *J. Chem. Soc., Dalton Trans.* **1975**, 1186.
(16) Barley, M. H.; Takeuchi, K. J.; Meyer, T. J. *J. Am. Chem. Soc.* **1986**, *108*, 5876.
(17) Epstein, I. R.; Kustin, K.; Warshaw, L. J. *J. Am. Chem. Soc.* **1980**, *102*, 3751.
(18) Uchiyama, S.; Muto, G.; Nozaki, K. *J. Electroanal. Chem. Interfacial Electrochem.* **1978**, *91*, 301.
(19) Hughes, M. N.; Shrimanker, K.; Wimbledon, P. E. *J. Chem. Soc., Dalton Trans.* **1978**, 1634.

0020-1669/88/1327-3279$01.50/0

to distinguish between the reactions of Fe^{II}(edta) and Fe^{III}(edta). A remarkable difference is the fact that Fe^{II}(edta) reacts with NO_2^- and NO(aq) to produce Fe^{II}(edta)NO, whereas Fe^{III}(edta) does not exhibit such reactions under similar conditions. Stopped-flow and *T*-jump measurements demonstrated that the reaction of Fe^{II}(edta) with NO is extremely fast and no kinetic data could be obtained by using these techniques. Similar findings were reported in the literature[20] and lower limits of 6×10^7 M^{-1} s^{-1} and 60 s^{-1} were predicted for k_1 and k_{-1}, respectively:

$$Fe^{II}(edta) + NO(aq) \underset{k_{-1}}{\overset{k_1}{\rightleftharpoons}} Fe^{II}(edta)NO \qquad (1)$$

Hishinuma et al.[21] reported the equilibrium constant $K_1 = 1 \times 10^6$ M^{-1}.

The reactions of Fe^{II}(edta) with $HONO/NO_2^-$ can be studied conveniently by using stopped-flow techniques. This reaction can be initiated either through the oxidation of NO(aq) by O_2 to various NO_x species (including HONO and NO_2^-) or through the reaction with $NaNO_2$. The observed reaction strongly depends on the pH and O_2 content of the solution since these parameters determine the relative composition of the NO_x system. It is therefore important to separate the various processes that lead to the formation of Fe(edta)NO, since a similar situation may occur during the catalyzed absorption of NO from flue gases in the presence of O_2.

UV–vis spectral studies indicated that Fe(edta)NO exhibits absorption maxima at 635 (128), 430 (685), and 340 nm (905 M^{-1} cm^{-1}). These values are in close agreement with those reported elsewhere.[11,20,21] Similar spectra are produced when Fe^{II}(edta) is treated with an excess of $NaNO_2$, although the band at 340 nm is then completely covered by an intensive absorption resulting from the partial formation of Fe^{III}(edta), which exhibits a band at 255 nm (8500 M^{-1} cm^{-1}). Along with this observation goes the fact that under such conditions only 50% of the Fe^{II}(edta) is converted to Fe^{II}(edta)NO, the rest being converted to Fe^{III}(edta). The formation of Fe^{III}(edta) is not observed during the reaction of Fe^{II}(edta) with NO(aq). It follows that the degree of conversion of Fe^{II}(edta) to Fe^{II}(edta)NO will depend on the $NO(aq)/NO_2^-$/HONO composition of the solution, which in turn depends on the pH, $[O_2]$, and way in which the solution was prepared.[12] It was found throughout the study that, in the absence of O_2, the reaction of Fe^{II}(edta) with an excess of $NaNO_2$ always produces Fe^{III}(edta) and Fe^{II}(edta)NO in the ratio 1:1. In the case of a mixture of NO and NO_2^-, Fe^{II}(edta) will react rapidly with the available NO followed by a slower step during which 50% of the remaining $[Fe^{II}(edta)]$ is converted to Fe^{II}(edta)NO. Experiments with nitrite at low pH indicated an immediate absorbance increase at 430 nm upon mixing in the stopped-flow instrument, which could be assigned to the reaction with NO(aq). In acidic medium, nitrite disproportionates into NO and NO_3^-, which accounts for the partial presence of NO under such conditions.[12] In order to prevent this complication, the Fe^{II}(edta) stock solutions rather than the nitrite solutions were acidified prior to mixing.

An important aspect of this study concerns the coordination geometry of Fe^{II}(edta). A 10^{-3} M 1:1 mixture of $FeCl_2$ and $Na_2(H_2edta)$ results in a pH of 2.76. This means that 1.74×10^{-3} M H^+ is released during complex formation, and the species Fe^{II}(edta) and Fe^{II}(Hedta) are present in the ratio 2.3:1. A pH titration of this mixture with NaOH indicates no deprotonation steps and is characteristic for the neutralization of free acid. On the addition of 1 equiv of NaOH a pH of 3.04 is reached, which corresponds to a composition of Fe^{II}(edta) and Fe^{II}(Hedta) in the ratio 9:1. The neutralization point is reached at 2 equiv of base, where the pH increases drastically from below 5 to above 9. It follows from this titration that the partial formation of the ring-opened, protonated complex Fe^{II}(Hedta) occurs at pH <3. Furthermore, there is no evidence for a coordinated water molecule with a pK_a value lower than 9.5. A similar titration could not be performed with $FeSO_4$ or in sulfate medium due to the interference of the formation of HSO_4^- at low pH.

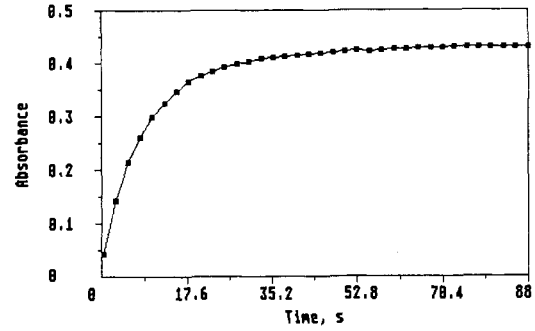

Figure 1. Typical absorbance/time plot for the formation of Fe^{II}(edta)NO in the presence of an excess of Fe^{II}(edta). Conditions: $[Fe^{II}(edta)] = 5 \times 10^{-3}$ M; [total NO_2^-] $= 5 \times 10^{-4}$ M; pH 3.14; temperature 25 °C; ionic strength 0.5 M; wavelength 430 nm; optical path length 1 cm.

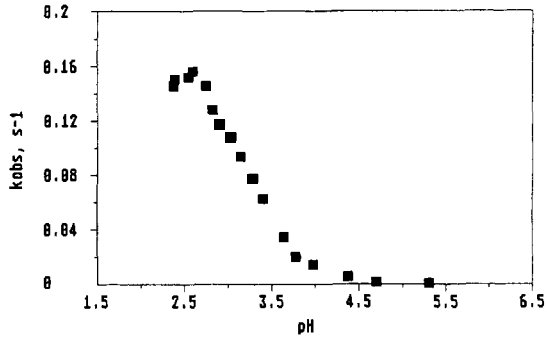

Figure 2. pH dependence of k_{obsd} for the data in Table I.

Table I. pH Dependence of k_{obsd} for the Reaction[a] Fe^{II}(edta) + $HONO/NO_2^- \rightarrow Fe^{II}$(edta)NO

pH	k_{obsd},[b] s^{-1}	pH	k_{obsd},[b] s^{-1}
2.38[c]	0.145 ± 0.006	2.91[c]	0.117 ± 0.003
2.39[c]	0.15 ± 0.01	3.04[c]	0.108 ± 0.005
2.56[c]	0.152 ± 0.003	3.14[c]	0.093 ± 0.008
2.61[c]	0.156 ± 0.005	3.29[c]	0.077 ± 0.003
2.75[c]	0.145 ± 0.004	3.4[c]	0.062 ± 0.003
2.83[c]	0.128 ± 0.005		
3.64[d]	0.034 ± 0.003	4.38[d]	0.0049 ± 0.0005
3.78[d]	0.0194 ± 0.0005	4.70[d]	0.00048 ± 0.0005
3.98[d]	0.0143 ± 0.0003	5.30[d]	0.00048 ± 0.0005

[a] Conditions: $[Fe^{II}(edta)] = 5 \times 10^{-3}$ M; [total NO_2^-] $= 5 \times 10^{-4}$ M; temperature 25 °C; ionic strength 0.5 M. [b] Mean value of five kinetic runs. [c] pH adjusted with H_2SO_4 and NaOH. [d] Acetic acid/acetate buffer 0.1 M.

Kinetic Measurements. A detailed kinetic study of the Fe^{II}(edta)/NO_2^-/HONO system was undertaken at 25.0 °C and 0.5 M ionic strength. The reactions were studied under pseudo-first-order conditions, i.e. with either Fe^{II}(edta) or $HONO/NO_2^-$ in at least 10-fold excess. Under these conditions, systematic concentration and pH dependence studies were undertaken.

When Fe^{II}(edta) is used in excess, the absorbance/time plots at 430 nm are typical for a pseudo-first-order reaction (see Figure 1) and the corresponding ln $(A_\infty - A_t)$ versus *t* plots are linear for at least 2–3 half-lives of the reaction. The observed rate constant, k_{obsd}, increases linearly with $[Fe^{II}(edta)]$ and exhibits a substantial pH dependence (see Table I for a summary of the kinetic data). Acetate buffers were used at pH >3.4, and control experiments in the absence of buffer indicate no influence of the buffer on the observed rate constant, although the pH of the solution does drift under such conditions. A plot of k_{obsd} versus pH at constant $[Fe^{II}(edta)]$ (Figure 2) reaches a maximum at pH

(20) Littlejohn, D.; Chang, S. G. *J. Phys. Chem.* **1982**, *86*, 537.
(21) Hishinuma, Y.; Kaji, R.; Akimoto, H.; Nakajima, F.; Mori, T.; Kamo, T.; Arikawa, Y.; Nozawa, S. *Bull. Chem. Soc. Jpn.* **1979**, *52*, 2863.
(22) Seinfeld, J. H. *Atmospheric Chemistry and Physics of Air Pollution*; Wiley: New York, 1985.

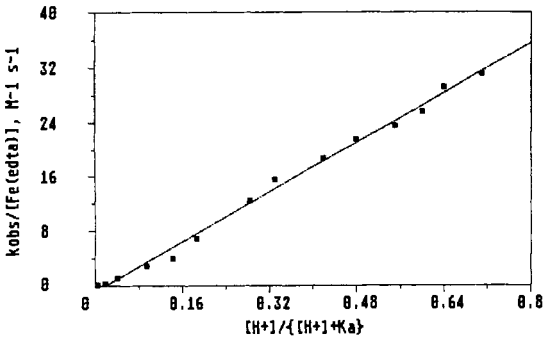

Figure 3. Plot of $k_{obsd}/[Fe(edta)]$ versus $[H^+]/([H^+] + K_a)$ for the data in Table I according to eq 4.

2.5 and is characteristic for a process involving an acid–base equilibrium. The decrease in k_{obsd} observed at pH <2.5 is presumably due to the partial protonation, accompanied by chelate ring opening, of the Fe^{II}(edta) species as discussed above. The reaction scheme outlined in (2) can account for the observed pH

$$\begin{aligned} HONO &\overset{K_a}{\rightleftharpoons} NO_2^- + H^+ \\ HONO + Fe^{II}(edta) &\xrightarrow{k_2} \text{products} \\ NO_2^- + Fe^{II}(edta) &\xrightarrow{k_3} \text{products} \end{aligned} \tag{2}$$

dependence. The reaction products consist of Fe^{II}(edta)NO and Fe^{III}(edta) in the ratio 1:1. In (2) k_2 and k_3 represent overall second-order rate constants; the detail of the mechanism and the nature of the rate-determining step will be discussed. For the mechanism outlined in (2), k_{obsd} can be expressed as in (3), which

$$k_{obsd} = \left(\frac{k_2[H^+] + k_3K_a}{[H^+] + K_a} \right) [Fe^{II}(edta)] \tag{3}$$

$$k_{obsd} = k_2[H^+][Fe^{II}(edta)]/([H^+] + K_a) \tag{4}$$

$$[Fe^{II}(edta)]/k_{obsd} = 1/k_2 + K_a/k_2[H^+] \tag{5}$$

reduces to (4) since $k_3 \ll k_2$ (k_{obsd} approaches zero at pH >4.5). Equation 4 can be rewritten as in (5), from which it follows that a plot of $[Fe^{II}(edta)]/k_{obsd}$ versus $[H^+]^{-1}$ should be linear with intercept k_2^{-1} and slope K_a/k_2. This is indeed the case for the data in the pH range 2.6–3.4, and the resulting values are $K_a = (1.0 \pm 0.2) \times 10^{-3}$ M and $k_2 = 44 \pm 4$ M^{-1} s^{-1}. This value of K_a is in excellent agreement with that obtained from a titration of $NaNO_2$ with H_2SO_4 at 25 °C and 0.5 M ionic strength, viz. $(1.0 \pm 0.1) \times 10^{-3}$ M. The data in Figure 2 can be fitted over a wider pH range by plotting $k_{obsd}/[Fe^{II}(edta)]$ versus $[H^+]/([H^+] + K_a)$ and using the directly determined value of K_a. Such a plot is given in Figure 3 for the pH range 2.6–5.3, and the resulting slope of 45 ± 3 M^{-1} s^{-1} is in excellent agreement with that obtained from the inverse plot procedure described above.

These data-fitting procedures clearly demonstrate that $k_2 \gg k_3$. This presumably correlates very well with the redox potentials of HONO and NO_2^-, viz. 0.99 and −0.46 V, respectively.[23] The rate-determining step therefore involves reduction of HONO and NO_2^- by Fe^{II}(edta) to produce Fe^{III}(edta) and NO, which subsequently reacts rapidly with Fe^{II}(edta) to produce Fe^{II}(edta)NO. In this way we can also account for the formation of Fe^{II}(edta)NO and Fe^{III}(edta) in the ratio 1:1. The rate-determining step in (2) can therefore be formulated as in (6).

$$\begin{aligned} HONO + Fe^{II}(edta) &\xrightarrow{k_2} Fe^{III}(edta) + NO + OH^- \\ Fe^{II}(edta) + NO &\xrightarrow{\text{fast}} Fe^{II}(edta)NO \end{aligned} \tag{6}$$

When nitrite is used in excess, the absorbance/time plots deviate from first-order behavior. This deviation strongly depends on pH and [total nitrite]. The absorbance/time plots consist of an initial first-order and subsequent zero-order section. Typical plots are presented in Figure 4 which were recorded under different pH conditions. The curves exhibit an increasing contribution from the linear zero-order section with decreasing pH. The zero-order curve exhibits a sudden inflection when the final absorbance is reached. The plots indicate that the initial stage of the reaction exhibits good first-order kinetics but that toward the end of the reaction at high pH, or even sooner at low pH, a zero-order process is rate-determining. The absorbance/time curves were converted to concentration/time curves, and the reaction rate, expressed as $-d[Fe(edta)]/dt$ (calculated from the [Fe(edta)NO] produced during the reaction), was calculated as a function of [Fe(edta)]. A plot of $-d[Fe(edta)]/dt$ versus [Fe(edta)] during the course of the reaction (see Figure 5) enables the calculation of the first-order rate constant from the slope and the zero-order rate constant from the intercept. Such plots exhibit an increasing intercept and a decreasing slope when the zero-order contribution increases at lower pH and higher [total NO_2^-]. Under limiting conditions, Figure 5 exhibits no intercept, i.e. where the zero-order contribution is negligible, or only an intercept and no slope, i.e. where the first-order contribution is negligible. This adopted procedure enables a consistent and reliable separation of the two rate constants.

A summary of the calculated zero- and first-order rate constants as a function of pH and [total NO_2^-] is given in Tables II and III, respectively. These rate constants increase with increasing [total NO_2^-] and decreasing pH, which can be expressed in terms of [HONO]. The observed zero-order rate constant k_A exhibits a linear dependence on $[HONO]^2$ as demonstrated by the plot of log k_A versus log [HONO] in Figure 6. It follows from the

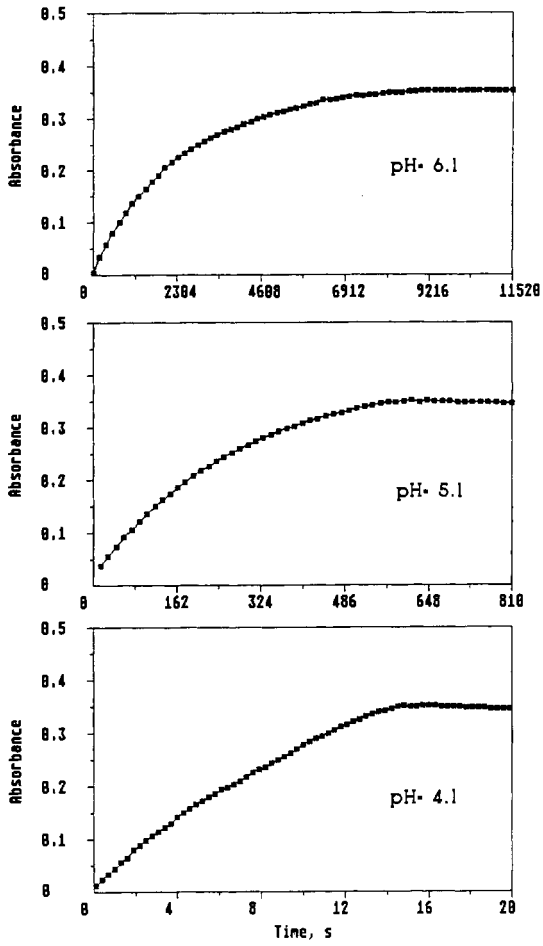

Figure 4. Typical absorption/time plots for the formation of Fe^{II}(edta)NO in the presence of an excess of nitrite as a function of pH. Conditions: $[Fe(edta)] = 1 \times 10^{-3}$ M; [total NO_2^-] $= 1 \times 10^{-2}$ M; temperature 25 °C; ionic strength 0.5 M; wavelength = 430 nm; optical path length = 1 cm.

(23) *Handbook of Chemistry and Physics*, 62nd ed.; CRC: Boca Raton, FL, 1981; p D-133.

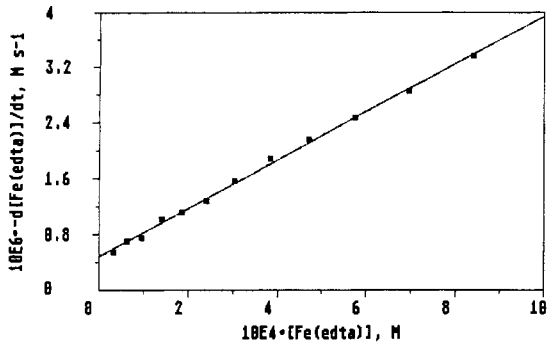

Figure 5. Plot of $-d[Fe^{II}(edta)]/dt$ versus $[Fe^{II}(edta)]$ as a function of time to calculate k_A and k_B according to eq 10. Conditions: [Fe(edta)] = 1×10^{-3} M; [total NO_2^-] = 1×10^{-2} M; temperature 25 °C; ionic strength 0.5 M; wavelength 430 nm; pH 5.1.

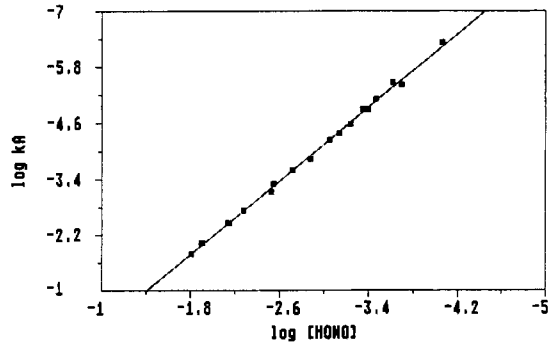

Figure 6. Plot of log k_A versus log [HONO] for the data in Table II.

Table II. Values of the Pseudo-Zero-Order Rate Constant k_A as a Function of [total NO_2^-] and pH[a]

[total NO_2^-], M	pH	k_A, M s^{-1}
0.01	5.06[b]	$(0.47 \pm 0.03) \times 10^{-6}$
0.03	5.10[b]	$(3.6 \pm 0.4) \times 10^{-6}$
0.05	5.17[b]	$(7.9 \pm 1.9) \times 10^{-6}$
0.07	5.20[b]	$(1.3 \pm 0.1) \times 10^{-5}$
0.01	4.70[b]	$(0.38 \pm 0.02) \times 10^{-5}$
0.02	4.70[b]	$(1.35 \pm 0.04) \times 10^{-5}$
0.03	4.71[b]	$(2.7 \pm 0.8) \times 10^{-5}$
0.05	4.75[b]	$(6.0 \pm 0.4) \times 10^{-5}$
0.01	4.11[b]	$(0.43 \pm 0.02) \times 10^{-4}$
0.02	4.16[b]	$(1.5 \pm 0.1) \times 10^{-4}$
0.03	4.17[b]	$(2.6 \pm 0.2) \times 10^{-4}$
0.05	4.23[b]	$(5.2 \pm 0.1) \times 10^{-4}$
0.01	3.39[c]	$(0.75 \pm 0.02) \times 10^{-3}$
0.02	3.25[c]	$(3.5 \pm 0.05) \times 10^{-3}$
0.03	3.15[c]	$(9.58 \pm 0.02) \times 10^{-3}$
0.01	2.70[c]	$(0.18 \pm 0.02) \times 10^{-2}$
0.01	2.62[c]	$(0.36 \pm 0.01) \times 10^{-2}$
0.02	2.82[c]	$(0.97 \pm 0.03) \times 10^{-2}$
0.03	2.98[c]	$(1.65 \pm 0.08) \times 10^{-2}$

[a] Mean k_A data resulting from variation of $[Fe^{II}(edta)] = (1-3) \times 10^{-3}$ M with [total NO_2^-] in 10-fold excess; temperature 25 °C, ionic strength 0.5 M. [b] Acetic acid/acetate buffer 0.1 M. [c] pH adjusted with H_2SO_4 and NaOH.

latter that the slope is 1.97 ± 0.02 with an intercept of 62 ± 12 M^{-1} s^{-1}. The mechanism outlined in (7) is suggested to account for the observed dependence, and the corresponding rate expression is given in (8). It follows from the intercept in Figure 6 that k_4

$$\begin{aligned} \mathrm{HONO} + \mathrm{HONO} &\xrightarrow{k_4} \mathrm{NO^+} + \mathrm{OH^-} + \mathrm{HONO} \\ \mathrm{Fe^{II}(edta)} + \mathrm{NO^+} &\xrightarrow{\text{fast}} \mathrm{Fe^{III}(edta)} + \mathrm{NO} \\ \mathrm{Fe^{II}(edta)} + \mathrm{NO} &\xrightarrow{\text{fast}} \mathrm{Fe^{II}(edta)NO} \end{aligned} \tag{7}$$

$$\begin{aligned} k_A &= -d[\mathrm{Fe(edta)}]/dt \\ &= 2k_4[\mathrm{HONO}]^2 \end{aligned} \tag{8}$$

Table III. Values of the Pseudo-First-Order Rate Constant k_B as a Function of [total NO_2^-] and pH[a]

[total NO_2^-], M	pH	k_B, s^{-1}
0.01	6.09	$(0.44 \pm 0.02) \times 10^{-3}$
0.05	6.16	$(2.34 \pm 0.08) \times 10^{-3}$
0.10	6.21	$(4.41 \pm 0.09) \times 10^{-3}$
0.15	6.21	$(6.7 \pm 0.1) \times 10^{-3}$
0.01	5.06	$(0.35 \pm 0.08) \times 10^{-2}$
0.03	5.10	$(1.20 \pm 0.06) \times 10^{-2}$
0.05	5.17	$(1.95 \pm 0.07) \times 10^{-2}$
0.07	5.20	$(2.6 \pm 0.2) \times 10^{-2}$
0.01	4.70	$(1.12 \pm 0.03) \times 10^{-2}$
0.02	4.70	$(2.5 \pm 0.7) \times 10^{-2}$
0.03	4.71	$(3.5 \pm 0.5) \times 10^{-2}$
0.01	4.11	$(5.9 \pm 0.5) \times 10^{-2}$
0.02	4.16	$(1.10 \pm 0.03) \times 10^{-1}$

[a] Mean k_B data resulting from variation of $[Fe^{II}(edta)] = (1-3) \times 10^{-3}$ M with [total NO_2^-] in 10-fold excess: temperature 25 °C, ionic strength 0.5 M; acetic acid/acetate buffer 0.1 M.

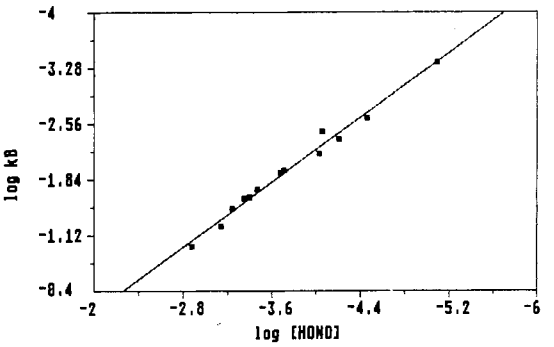

Figure 7. Plot of log k_B versus log [HONO] for the data in Table III.

$= 31 \pm 6$ M^{-1} s^{-1}. The observed first-order rate constant k_B exhibits a linear dependence on [HONO] as demonstrated by a plot of log k_B versus log [HONO] in Figure 7. This plot exhibits a slope of 1.04 ± 0.04 and an intercept of 90 ± 16 M^{-1} s^{-1}. The suggested mechanism is outlined in (6) and the corresponding rate expression presented in (9). It follows that $k_B = 2k_2[\mathrm{HONO}]$,

$$\begin{aligned} -d[\mathrm{Fe(edta)}]/dt &= k_B[\mathrm{Fe(edta)}] \\ &= 2k_2[\mathrm{Fe(edta)}][\mathrm{HONO}] \end{aligned} \tag{9}$$

such that $k_2 = 45 \pm 8$ M^{-1} s^{-1}. This value for k_2 is in excellent agreement with that calculated above from the data for the reaction in the presence of an excess of $Fe^{II}(edta)$.

The overall mechanism, which consists of the reactions in (2), (6), and (7), can account for the mixed order dependence observed when nitrite is used in excess, on the basis of the overall rate equation in (10). At high pH and low nitrite concentration, the

$$\begin{aligned} -d[\mathrm{Fe(edta)}]/dt &= k_A + k_B[\mathrm{Fe(edta)}] \\ &= 2k_4[\mathrm{HONO}]^2 + 2k_2[\mathrm{Fe(edta)}][\mathrm{HONO}] \end{aligned} \tag{10}$$

k_2 step is rate-determining and mainly the pseudo-first-order behavior is observed. However, as the reaction proceeds, $[Fe^{II}(edta)]$ decreases and the rate of the overall process in (6) decreases to the point that the zero-order path contributes substantially. The latter path will play a more important role at lower pH and higher nitrite concentrations, i.e. where [HONO] is significant. Under extreme conditions, this path will represent the major contribution and the observed kinetic trace will approach that of a zero-order process. Furthermore, in the presence of an excess of $Fe^{II}(edta)$, the rate of the k_2 process will not decrease with decreasing $[Fe^{II}(edta)]$ and the process in (6) represents the only reaction path, with no deviation in the first-order behavior. In fact, [HONO] is too low under such conditions to contribute significantly to the process via the reaction in (7). In this respect, we must emphasize that the nature of the reactive species produced by HONO is at present unknown. We have formulated this species

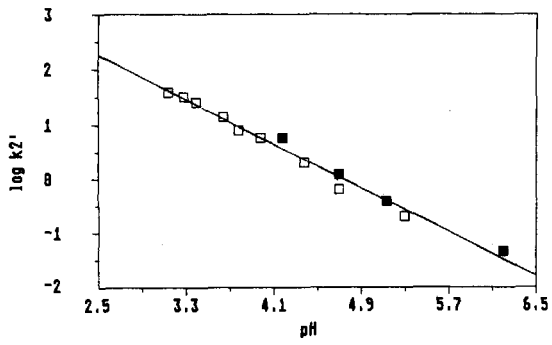

Figure 8. Comparison of the k_2' data obtained for Fe(edta) (□) and NO_2^- (■) in excess where $k_2' = k_{obsd}/[Fe^{II}(edta)] = k_2[H^+]/([H^+] + K_a)$ (see eq 4) or $k_2' = k_B/2[\text{total } NO_2^-] = k_2[H^+]/([H^+] + K_a)$ (see eq 9).

as NO^+ on the basis of recent reports in the literature,[14,19] but it might be N_2O_3, which will react in a similar manner in the subsequent non-rate-determining steps. It is encouraging to note that the values of k_2, obtained in two completely different ways, are so similar. A comparison of these data as a function of pH is presented in Figure 8. The data for the process with excess $Fe^{II}(edta)$ is expressed as $k_{obsd}/[Fe^{II}(edta)]$ and for the reaction with excess nitrite as $k_B/2[\text{total } NO_2^-]$ according to eq 4 and 9, respectively. The pH dependence of these data arises solely from the fraction of nitrite present as HONO, which decreases with increasing pH.

A comparison of our results for the $Fe^{II}(edta)/HONO/NO_2^-$ system with those reported in the literature reveals that although the studies were carried out under different conditions, the results correlate well. Uchiyama et al.[18] followed the formation of $Fe^{II}(edta)NO$ using a method referred to as concentration-step controlled-potential electrolysis. They worked with an excess of $Fe^{II}(edta)$ and therefore only observed the pseudo-first-order reaction path. We have extrapolated a second-order rate constant (k_2) of 50 M^{-1} s^{-1} from their data, which is very close to that reported in this study. Shearer[11] studied the system in detail but used a different procedure for the calculation of the rate constants. The second-order rate constants extrapolated from his data with use of plots of log k_{obsd} vs log [HONO] are $k_4 = 11$ M^{-1} s^{-1} and $k_2 = 41$ M^{-1} s^{-1}, once again in fair agreement with our findings. His suggested mechanism is very similar to ours except for his choice of NO_2^- as the reactive species. It is also important to note that he was unable to detect the square dependence of the pseudo-zero-order rate constant on [HONO] from his limited pH-dependence study.

The results of this study clearly demonstrate how the formation of $Fe^{II}(edta)NO$ can occur along different reaction routes depending on the experimental conditions employed. In the absence of oxygen, $Fe^{II}(edta)$ will pick up NO on a microsecond time scale. In the presence of oxygen, NO will be partially oxidized to $HONO/NO_2^-$ (as evidenced by the characteristic fingerprint spectrum observed for HONO at low pH in the range 300–400 nm[24]) and $Fe^{II}(edta)$ to $Fe^{III}(edta)$. Under such conditions, HONO is the reactive species and is responsible either for the formation of NO^+ (or N_2O_3) or for the formation of NO via the oxidation of $Fe^{II}(edta)$ to $Fe^{III}(edta)$. It follows that the complete process is controlled by $[O_2]$, pH, and [total NO_2^-] since these factors control the balance between the various reaction routes.

The rapid formation of $Fe^{II}(edta)NO$ is most probably due to the presence of a labile water molecule in the coordination sphere of $Fe^{II}(edta)$. Although we have no direct evidence for the presence of such a water molecule, the observed reactivity, as well as studies on the closely related $Ru^{III}(edta)$ system,[25-27] suggest this to be the case. A ring-opened edta ligand can via hydrogen bonding labilize the coordinated water molecule or enable an associative attack of the entering ligand. Protonation of such a species (at pH <3 in our case) will decrease this interaction and account for the decrease in reactivity observed under such conditions. In this respect it is important to note that recent Mössbauer spectroscopic studies of the $Fe^{II}(edta)$ system[28] suggest the formation of a protonated species at pH 2.5. It is therefore quite realistic to formulate the complex as $Fe^{II}(edta)H_2O$, in which the edta ligand occupies five coordination sites and the ring-opened edta ligand is protonated at pH <3.

Acknowledgment. We gratefully acknowledge financial support from the Deutsche Forschungsgesellschaft, the Fonds der Chemischen Industrie, and the Max-Buchner Forschungsstiftung.

Registry No. $Fe^{II}(edta)$, 21393-59-9; HONO, 7782-77-6; NO_2^-, 14797-65-0.

(24) Stockwell, W. R.; Calvert, J. G. *J. Photochem.* **1978**, *8*, 193.
(25) Matsubara, T.; Creutz, C. *J. Am. Chem. Soc.* **1978**, *100*, 6255.
(26) Matsubara, T.; Creutz, C. *Inorg. Chem.* **1979**, *18*, 1956.
(27) Bajaj, H. C.; van Eldik, R. *Inorg. Chem.*, in press.
(28) Marton, A.; Sükösd-Rozlosnik, N.; Vértes, A.; Nagy-Czakó, I.; Burger, K. *Inorg. Chim. Acta* **1987**, *137*, 173.

Contribution from the Department of Chemistry,
The University of North Carolina at Chapel Hill, Chapel Hill, North Carolina 27514

Redox Properties and Ligand Loss Chemistry in Aqua/Hydroxo/Oxo Complexes Derived from *cis*- and *trans*-$[(bpy)_2Ru^{II}(OH_2)_2]^{2+}$

John C. Dobson and Thomas J. Meyer*

Received December 14, 1987

Electrochemical studies on the cis and trans isomers of $[(bpy)_2Ru^{II}(OH_2)_2]^{2+}$ (bpy is 2,2'-bipyridine) as a function of pH in aqueous solution have revealed the existence of a series of pH-dependent redox couples that interconvert oxidation states II → VI. The electrochemical data give insight into the relative stabilities of the cis and trans isomers as well the stabilities of individual oxidation states. In acidic solution, oxidation state VI for the cis complex is unstable with respect to ligand loss and the resulting Ru(VI) complex is unstable with respect to reduction to Ru(III). Comparisons with redox potentials for related couples allow a qualitative assessment to be made concerning the role of electronic structure in determining the magnitudes of redox potentials and of the possible use of monomeric aqua/hydroxo/oxo couples as four-electron oxidants for the catalytic oxidation of water to molecular oxygen.

Introduction

The oxidation of water to molecular oxygen is a problem of both technological and fundamental interest. One of our concerns has been with the design of molecular catalysts for water oxidation that could conceivably be integrated into more complex photochemical or electrochemical energy conversion systems.[1] We and others have shown that the μ-oxo ion $[(bpy)_2(OH_2)RuORu(OH_2)(bpy)_2]^{4+}$ (bpy is 2,2'-bipyridine) and its derivatives are

(1) See, for example: (a) *Energy Resources through Photochemistry and Catalysis*; Gratzel, M., Ed.; Academic: New York, 1983. (b) *Chemically Modified Surfaces in Catalysis and Electrocatalysis*; Miller, J. S., Ed.; American Chemical Society: Washington, DC, 1982.

0020-1669/88/1327-3283$01.50/0